Simulations of Runaway Electron Generation including Hot-Tail Effect

H Nuga[1], M Yagi[2], A Fukuyama[3]

[1]National Institute for Fusion Science, Toki, Japan
[2]National Institutes for Quantum and Radiological Science and Technology, Rokkasho, Japan
[3]Department of Nuclear Engineering, Kyoto University, Kyoto, Japan

E-mail: nuga.hideo@nifs.ac.jp

December 2016

Abstract. The hot-tail (H-T) effect in disruptions with impurity injection is considered. The contribution of H-T effect on runaway electron (RE) current, which arises from fast thermal quench, is studied using two-dimensional Fokker-Planck simulation. It is found that in a high density plasma, the total RE current is reduced owing to its high collisionality. We also found that if the thermal quench is fast enough to invoke the H-T effect, the effect produces more seed REs than that excluding H-T effect even in high density plasmas. In high density region ($n_e \sim 10^{21}$ m^{-3}) with fast thermal quench, nevertheless the increment of the seed REs due to H-T effect is generally small (tens of mili amperes), the increment of the total RE current reached to 2 MA owing to the avalanche effect.

Keywords: Disruption, Runaway electrons Submitted to: *Nucl. Fusion*

1. Introduction

Disruption is one of the most serious events in tokamaks, since it induces huge electromagnetic force to the device and generates high-energy REs which may cause the damage of plasma facing components [1]. Especially in a high current tokamak such as ITER, since the RE current is considered to reach multi-mega amperes. the damage to device surfaces should be avoided and mitigated. To avoid the damage of the first wall by REs, several strategies are proposed [2, 3] such as the RE deconfinement [4] and the position control of RE beam [5]. The collisional suppression [6] is one of the strategies. This strategy aims to suppress the RE generation by the rapid increase of electron density. Massive Gas Injection (MGI) is one of the most popular and demonstrated method [7–13] to rise the electron density in disruptive plasmas. Additionally, Killer Pellet Injection (KPI) [14,15], Shattered Pellet Injection (SPI), and SHell Pellet Injection (SHPI) [16, 17] are also used for the methods of the collisional suppression. The collisional suppression, however, tends to shorten the thermal quench duration and may enhance the primary RE generation through the so-called "hot-tail (H-T) effect" [18,19].

The H-T effect, or "burst generation" [20], is the phenomenon that the fast thermal quench enhances the primary RE generation. The mechanism comes from the incomplete thermalization owing to the fact that the collisionality decreases with the increasing the velocity. If the bulk plasma temperature drops rapidly before high-velocity electrons slow down, the high velocity tail of the electron distribution function, namely H-T, is formed. The presence of the H-T electrons leads to the significant increase of the REs. This effect has been discussed in several simulations [18, 21–23] and experiments [15, 24, 25].

Aim of this paper is the estimation of the RE current generated in the disruption mitigating plasma including H-T effect. To include the effect, we use two-dimensional Fokker-Planck simulation. In the present analysis, the primary RE generation rate is evaluated by the electron momentum distribution function obtained by using Fokker-Planck code TASK/FP [26–28]. Evolutions of the RE generation and the induced electric field are calculated self-consistently. Additionally, the drop of the plasma temperature and the increase of the electron density and the effective charge during thermal quench owing to impurity injection are implemented simply.

In our simulation results, the RE current generation is suppressed with the increase of the electron density as expected. Moreover, we also find that if the H-T effect is invoked, much more RE current is generated than that excluding H-T effect even in high density region ($n_e \sim 10^{21}$ m^{-3}). In such a high density region, even though the increment of the primary RE current due to H-T effect is very small (~ 50 mA), the increment of total RE current reaches to 2 mega-ampere owing to avalanche effect [29–31]. The H-T RE generation depends on the electron density during the H-T RE generation phase, which appears earlier in time than the bulk primary RE generation. Therefore the time scale of the density rise by impurity injection is important for RE current estimation.

The rest of this paper is organized as follows. Models of induced electric field,

RE generation rate, thermal quench, and increase of the electron density and effective charge are explained in Sec. 2. Introduction of the calculation parameters is provided in Sec. 3. Numerical result with slower and faster density increase cases are shown in Sec. 3.1 and 3.2. The validation of the definition of the primary RE generation rate is discussed in Sec. 4. Conclusion is provided in Sec. 5.

2. Basic equations

In this section, the induced toroidal electric field, the primary and secondary RE generation rates, the thermal quench of bulk plasma, and the increase of electron and ion densities and the effective charge are modeled. In addition, the Fokker-Planck equation, which is the governing equation of the electron momentum distribution function is expressed.

2.1. Fokker-Planck equation

In the present simulation model, the primary RE generation rate is defined from the relativistic momentum distribution function, which obeys the Fokker-Planck equation:

$$\frac{\partial f_e}{\partial t} = -\nabla \cdot \left[-\overleftrightarrow{\boldsymbol{D}}_C \cdot \nabla f_e + \left(\boldsymbol{F}_C + \frac{q\boldsymbol{E}}{m_e} \right) f_e \right], \tag{1}$$

where ∇ is the derivative operator in momentum space (p, θ). They denote the momentum and the pitch angle, respectively. The collisional diffusion and friction terms, $\overleftrightarrow{\boldsymbol{D}}_C$ and $\boldsymbol{F}_C$, are determined by the weak relativistic isotropic background collision term [32, 33] with relativistic Maxwellian. The background temperature and density, which is required for the collision term, are modeled in Sec. 2.3. In our simulation code TASK/FP, the momentum space (p, θ) is divided by finite difference method and defined in the range of $0 < p < p_{\max}$, and $0 < \theta < \pi$. Additionally, the time evolution is solved by the full implicit method. The boundary value $p_{\max}$ is chosen to be $p_{\max}^2/2m \sim 1.5$ MeV. The validity of the choice is discussed in Sec. 4.

2.2. Electric field and RE generation rate

The induced toroidal electric field E obeys the following equations:

$$\frac{1}{r}\frac{\partial}{\partial r}\left(r\frac{\partial E}{\partial r} \right) = \mu_0 \frac{\partial}{\partial t} j, \tag{2}$$

$$j = \sigma_{\parallel} E + ecn_r, \tag{3}$$

$$\frac{dn_{rp}}{dt} = -\int_0^{p_{\max}} \frac{\partial f_e}{\partial t} d\boldsymbol{p}, \tag{4}$$

$$\frac{dn_{rs}}{dt} = n_r \frac{E/E_C - 1}{\tau_r \ln\Lambda} \sqrt{\frac{\pi\varphi}{3(Z_{\text{eff}}+1)}} \times \left(1 - \frac{E_C}{E} + \frac{4\pi(Z_{\text{eff}}+1)^2}{3\varphi(Z_{\text{eff}}+1)(E^2/E_C^2 + 4/\varphi^2 - 1)} \right)^{-1/2} \tag{5}$$

where $\tau_r = 4\pi\varepsilon_0^2 m_e^2 c^3/n_e q_e^4$, $\varphi = 1 - 1.46\epsilon^{1/2} + 1.72\epsilon$, ϵ is the inverse aspect ratio, and $E_C = n_e q_e^3 \ln\Lambda/4\pi\varepsilon_0^2 m_e c^2$ is the critical electric field, respectively. If the electric field is below the critical electric field, no RE generation occurs. The boundary condition for the electric field is obtained by the expression of E in vacuum region: $E(r) \propto \ln(r/b)$, where $r = b$ is the location of the wall. The parallel conductivity $\sigma_\parallel$ in eq. (3) is the Spitzer conductivity with neo-classical correction [34]. The current density in eq. (2) is given by the Ohm's law (eq. (3)). Here, the plasma current is divided into two components: the ohmic current $\sigma_\parallel E$ and RE current ecn_r. The total RE density n_r is obtained by $n_r = n_{rp} + n_{rs}$, where n_{rp} and n_{rs} are the primary and secondary RE densities, respectively. It is assumed that all of REs travel with the velocity of light.

The two kind of RE densities are obtained by eqs. (4) and (5). The primary RE generation rate is determined by calculating the flux of the electron momentum distribution function f_e through the boundary of momentum calculation domain: $0 < p < p_{\max}$. In the present paper, we choose the upper boundary as follow: $(p_{\max})^2/(2m_e) = E_{\max} \sim 1.5$MeV. This means that the electrons whose kinetic energy is greater than 1.5MeV are regarded as REs. Although some REs reach to the energy of several tens of MeV in disruptive plasmas, we calculate f_e only under 1.5MeV. This is because we focus on not RE distribution in high energy region but the number of REs generated in disruptions. The validity of the choice of $E_{\max}$ will be discussed in Sec. 4. Contrary to the primary RE generation rate, the secondary RE generation rate is given by a function [31] of n_r and E/E_C rather than the momentum distribution.

2.3. Thermal quench and impurity injection

To evaluate the induced toroidal electric field, the decay of the plasma temperature and the corresponding plasma conductivity are necessary. However, the behavior of the thermal quench is too complex so that it is difficult to construct a reasonable model in RE generation time scale. Thus, in order to simulate RE generation in disruptions, a simple model for the thermal quench is adopted in the present calculation. The decay of the background plasma temperature is given by a following model:

$$T(t,\rho) = (T_0(\rho) - T_f(\rho))\exp(-t/\tau_q) + T_f(\rho), \tag{6}$$

$$T_0(\rho) = (T_0(0) - T_0(1))(1-\rho^2)^2 + T_0(1), \tag{7}$$

$$T_f(\rho) = T_f(0)(1 - 0.9\rho^2), \tag{8}$$

where ρ is the normalized minor radius, τ_q denotes the time constant of the thermal quench, and T_0 and T_f are the pre- and post-quench plasma temperature. Here ions and electrons are assumed to have the same temperature.

The evolutions of electron and ions densities and the effective charge assuming impurity injection are also modeled. Usually, noble gases, such as neon or argon, are used for impurity injection. In the low temperature plasma ($\sim$ tens of eV), however, most of impurity ions are not fully ionized. Since the issue of ionization state of impurities is complex, to simplify our model, we introduce post-injection effective charge $Z_{\rm eff}^f$ and

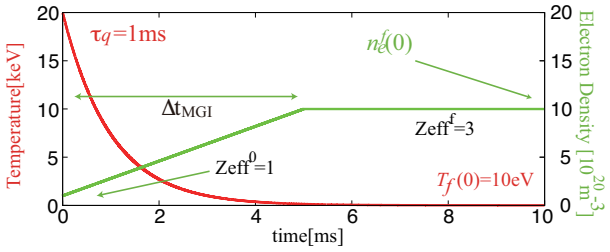

Figure 1. Model of thermal quench and density increase.

virtual impurity ion species, which has no electron-bound state. Additionally, the influence of the presence of the binding electron to the conductivity is also omitted. They satisfy the following relations:

$$n_e^f = n_e^0 + Z_i n_i^f, \quad Z_{\rm eff}^f = \frac{n_D + Z_i^2 n_i^f}{n_e^f}, \tag{9}$$

where, superscript 0 and f denote pre-quench and post-injection density or effective charge and subscript e, D and i denote ion species (electron, deuteron and impurity ion), respectively. In the following calculation, n_e^0, n_e^f, n_D, $Z_{\rm eff}^f$ are given, in contrary, n_i^f and Z_i are obtained to satisfy the relation. Similarly, evolution of the electron density is modeled as follows:

$$\begin{aligned} n_e(\rho) &= (n_e^f(\rho) - n_e^0(\rho))\frac{t}{\Delta t_{\rm I}} + n_e^0(\rho) \quad (t \le \Delta t_{\rm I}) \\ n_e(\rho) &= n_e^f(\rho) \qquad (\Delta t_{\rm I} < t), \end{aligned} \tag{10}$$

where $\Delta t_{\rm I}$ is the duration in which the electron density increases. The subscript I denotes Impurity injection. Impurity electron and ion have a same temperature, which is sufficiently lower than the bulk plasma temperature:

$$T_{\rm imp}(t,\rho) = 0.01T(t,\rho) + 0.99T_f(\rho). \tag{11}$$

The example of the evolution of the temperature and electron density are illustrated in Figure 1.

Our thermal quench and impurity models assume that the temperature and density keep radial dependence of electron and ion densities for simplicity. Actually, since impurities are transported from outer region or deposited locally, the thermal quench and the density rise should include the impurity transport for more accurate analysis.

3. H-T effect with impurity injection

The high density plasma ($\sim 10^{21} - 10^{22}$ m^{-3}) is desired to suppress the RE generation. Since the critical electric field E_C is proportional to the electron density, the secondary RE generation may be suppressed when the electric field is kept below the critical electric field E_C ($E/E_C < 1$). Moreover, even if $E/E_C > 1$, the high collisionality of the high density plasma may prevent from generating primary REs. If the H-T is formed,

however, the less collisional H-T electron may produce primary REs. In high current devices, since the secondary RE current becomes dominant, there is a possibility that the small increment of the primary RE current owing to H-T effect may be multiplied to non-negligible magnitude by the avalanche effect. Therefore we examine the density dependence of RE generation including H-T effect.

To clearly indicate the H-T effect, in the following section, we compare the simulation results including and excluding H-T effect. The difference between two cases is the model of the primary RE generation. The case excluding H-T effect adopts the model derived by Connor and Hastie [35] instead of eq. (4):

$$\frac{\tau_{th}}{n_e}\frac{dn_{rp}}{dt} = C_R(\alpha, Z_{\rm eff})\hat{E}^{-h(\alpha,Z_{\rm eff})} \times \exp\left(-\frac{\lambda(\alpha)}{4\hat{E}} - \sqrt{\frac{2}{\hat{E}}\Gamma(\alpha, Z_{\rm eff})}\right), \tag{12}$$

where, $\tau_{th} = 4\pi\varepsilon_0^2 m_e^2 v_{th}^3/n_e q_e^4 \ln\Lambda$, $\hat{E} = E/E_D$, $E_D = n_e q_e^3 \ln\Lambda/4\pi\varepsilon_0^2 m_e v_{th}^2$, $\alpha = \hat{E}mc^2/T$,

$$h(\alpha, Z_{\rm eff}) = \frac{1}{16(\alpha-1)}\left[\alpha(Z_{\rm eff}+1) - Z_{\rm eff} + 7 + 2\sqrt{\frac{\alpha}{\alpha-1}}(1+Z_{\rm eff})(\alpha-2)\right],$$

$$\lambda(\alpha) = 8\alpha\left(\alpha - \frac{1}{2} - \sqrt{\alpha(\alpha-1)}\right),$$

$$\Gamma(\alpha, Z_{\rm eff}) = \sqrt{\frac{(1+Z_{\rm eff})\alpha^2}{8(\alpha-1)}}\left[\frac{\pi}{2} - \arcsin\left(1-\frac{2}{\alpha}\right)\right],$$

and $C_R(\alpha, Z_{\rm eff})$ is an unknown constant of order unity in ϵ. In the present calculation, the unknown constant C_R is chosen to be 0.35. It was confirmed that if the thermal quench is sufficiently slow to suppress the H-T effect, both RE generation models give almost same results [28].

In the following calculation, we employ parameters tabulated in Table 1. Pre-quench electron and current density profiles are given by:

$$j(\rho) = j_0(1-\rho^2) \tag{13}$$

$$n_e^0(\rho) = (n_e^0(0) - n_e^0(1)) \times (1-\rho^2)^{0.67} + n_e^0(1). \tag{14}$$

Additionally, in the following calculation, we employ the time constant of the thermal quench $\tau_q = 1$ ms, the impurity injection duration $\Delta t_{\rm I} = 5$ ms, and the post-injection effective charge $Z_{\rm eff}^f = 3$. The typical thermal quench duration without impurity injection in ITER is roughly estimated in Ref. [36] as a function of the minor radius. The thermal quench consists of two stages, the first erosion of the central temperature and the subsequent fast break of edge thermal barrier, respectively. The subsequent fast quench, which spills out the $70-90\%$ of the total thermal energy, contributes to the H-T effect and the range of possible value of the fast quench is estimated to be $\Delta t = 0.3$ms-3ms in ITER. In our model, the duration which is required

Table 1. PLASMA PARAMETERS

Radii [m]	$R = 6.2$, $a = 2.0$, $b = 2.4$
Initial current [MA]	$I_P = 15$
Initial temperature [keV]	$T_0(0) = 20$, $T_0(1) = 2.0$
Post-quench temp. [eV]	$T_f(0) = 10$
Thermal quench time [ms]	$\tau_q = 1.0$
Pre-quench density	
on axis [m^{-3}]	$n_e^0(0) = 1.0 \times 10^{20}$
on edge [m^{-3}]	$n_e^0(1) = 1.0 \times 10^{19}$
Effective charge	$Z_{\rm eff}^0 = 1$, $Z_{\rm eff}^f = 3$
Ion species	Deuteron

to reduce $\sim 90\%$ of the thermal energy is $\Delta t \sim 2 - 3\tau_q$. Therefore, the value of thermal quench time $\tau_q = 1$ ms is within the realistic range. Actually, there is a possibility that the thermal quench duration becomes shorter than that of the rough estimation due to the impurity injection.

Moreover, in experiments in present devices [10, 37], the typical duration of the electron density rise is longer than that of thermal quench and the density increase lasts until the current quench begins. Therefore the value $\Delta t_{\rm I} = 5$ms can be see a valid value.

If we do not take the increment of the density into account, in our model, the ratio of τ_q and the electron-electron slowing down time for a few time of pre-quench thermal velocity $\tau_s^{ee}(2 - 3v_{\rm th0})$ could be regarded as a threshold value of the H-T effect [27, 28]. Namely, if the ratio satisfies $\tau_q/\tau_s^{ee}(3v_{\rm th0}) < 1$, the H-T effect may be excited. The value $\tau_q = 1$ms is sufficiently short to invoke the H-T effect for $n_e^f(0) = 10^{20}$ m^{-3} ($\tau_q/\tau_s^{ee}(3v_{\rm th0}) \sim 0.26$). Contrary, for high density case ($n_e^f = 10^{21}$ m^{-3}), the ratio becomes greater than a unit ($\tau_q/\tau_s^{ee}(3v_{\rm th0}) \sim 2.6$). In the following calculation, however, electron density increases in time. Therefore the ratio does not alway become the threshold value.

3.1. $\Delta t_{\rm I} = 5ms$ case

Figure 2 shows the $n_e^f(0)$ dependence of the (a) total, secondary, and (b) primary RE current. It is found that the increment of the electron density achieves to suppress the RE generation as expected. In low density region ($n_e^f(0) = 2 \times 10^{20}$ m^{-3}), most of pre-quench ohmic current is converted into RE current (total RE current: $I_{\rm RE} = 12.7$ MA). The primary RE current excluding H-T effect is $I_{\rm prim} = 3.96$ MA and that including H-T effect increases to $I_{\rm prim} = 4.85$ MA.

Figures 3 show the evolutions of plasma current, electric field, and two kinds of RE generation rates. From figs. 2-(a) and 3-(a), it is found that H-T effect does not multiply the total RE current in $n_e^f(0) = 2 \times 10^{20}$ m^{-3} case in spite of the increase of

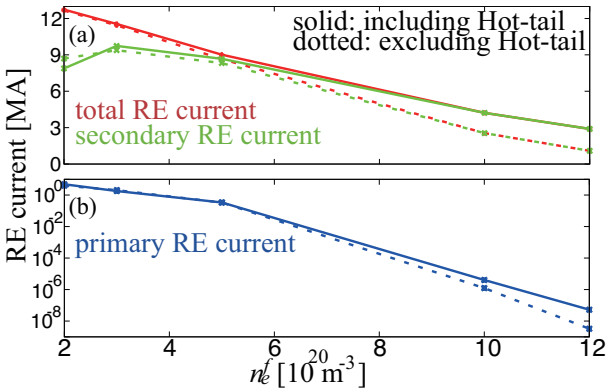

Figure 2. $n_e^f(0)$ dependence of the total, primary, and secondary RE current for $\tau_q = 1$ ms, $\Delta t_{\rm I} = 5$ms, and $Z_{\rm eff}^f = 3$.

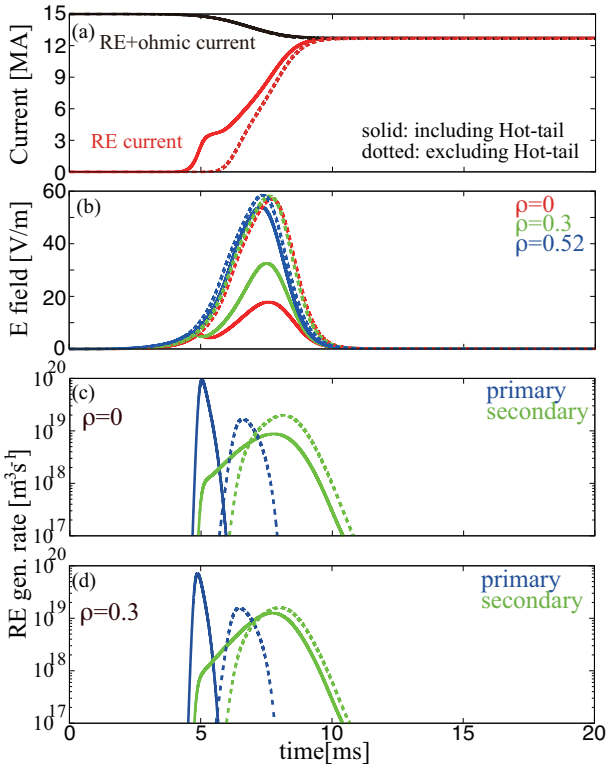

Figure 3. Evolutions of (a) total and RE current, (b) electric field on $\rho = 0$ and 0.3, and (c) RE generation rate on $\rho = 0$, and (d) $\rho = 0.3$ for $n_e^f(0) = 2 \times 10^{20}$ m^{-3}.

the primary RE current. This is because high primary RE generation rate due to H-T ($t \sim 5$ ms in figs. 3-(c,d)) reduces toroidal electric field (fig. 3-(b)) to conserve poloidal magnetic flux. Owing to the reduction of E field, the peak value of the secondary RE generation rate also decreases slightly (fig. 3-(c,d)). Figure 4 shows pre-quench ohmic and RE current density profiles. H-T effect multiplies RE current density slightly in $\rho < 0.4$ region, and reduces it slightly in $0.4 < \rho < 0.6$ region. In $0.4 < \rho < 0.6$ region,

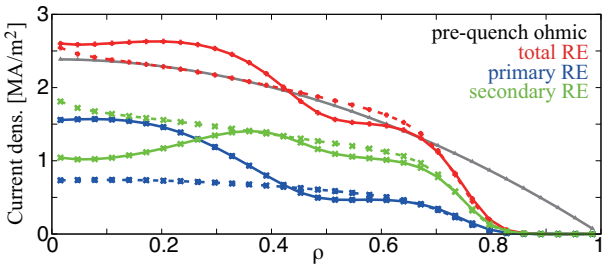

Figure 4. Current density profile for $n_e^f(0) = 2 \times 10^{20}$ m^{-3}. Solid and dotted curves are current density including and excluding H-T effect. Black, red, blue, and green curves denote pre-quench ohmic, total RE, primary RE, and secondary RE current density, respectively.

H-T effect reduces both of primary and secondary RE current density. This is because the electric field in $0.4 < \rho < 0.6$ region diffuses into inner region in order to fill the hollow of the electric field profile (fig. 3-(b)), which is made by the high primary RE generation in inner region ($\rho < 0.3$). Consequently, H-T effect has less influence to total RE current and RE current density profile when the most of pre-quench ohmic current is converted to RE current. Figure 5 shows the dynamic evolution of the electron momentum distribution function in two-dimensional momentum space at $t = 4 - 6$ms. It is found that fast electrons are not thermalized but form H-T and then they become REs.

On the other hand, in high density region (ex. $n_e^f(0) = 1.2 \times 10^{21}$ m^{-3}), RE current is suppressed to a few Mega Amperes. Especially, the suppression of the primary RE generation is remarkable (be suppressed to mili amperes). Although the high electron density succeeds to suppress the RE generation, the presence of the H-T effect makes the total RE current about three times in the region ($I_{\rm RE} = 1.09$ and 2.90 MA for excluding and including H-T effect cases). In this case, H-T effect enhances the primary RE current about 16 times ($I_{\rm prim} = 3.3$ mA to 52.8 mA), though the magnitude of the increment ($\Delta I_{\rm prim} = 49.6$ mA) is very small compared to total RE current. This small increment of the primary RE current is multiplied by the avalanche effect to 1.81 MA and total RE current becomes thrice. It means that a small increment of the primary RE current due to H-T effect may affect to the total RE current strongly when the secondary RE current is dominant.

Figure 6 shows the initial ohmic and RE current density profiles for $n_e^f(0) = 1.2 \times 10^{21}$ m^{-3} case. The RE current density profiles have a peak on axis rather than the initial profile. Furthermore, the H-T effect broadens the RE current profile. Figures 7 show the evolutions of (a) total and RE current, (b) induced electric field on axis and $\rho = 0.3$, and primary and secondary RE generation rates (c) on axis and (d) $\rho = 0.3$. From fig. 7 (c) and (d), it is found that the H-T effect makes a additional peak of the primary RE generation rate ($t \sim 5$ ms). This is because, H-T electrons can become REs easily rather than bulk electrons even with the weak electric field due to the low

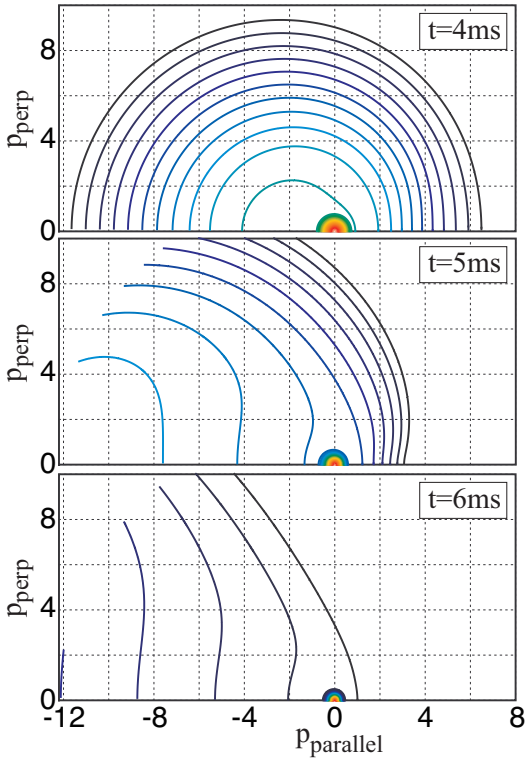

Figure 5. The electron momentum distribution functions in two dimensional momentum space at several time steps on $\rho = 0$ with $n_e^f(0) = 2 \times 10^{20}\mathrm{m}^{-3}$ and $\Delta t_I = 5$ ms. The horizontal and vertical axes denote the momentum in parallel and perpendicular directions, respectively. These values are normalized to pre-quench thermal momentum $p_{th0} = \sqrt{mT_0(0)}$.

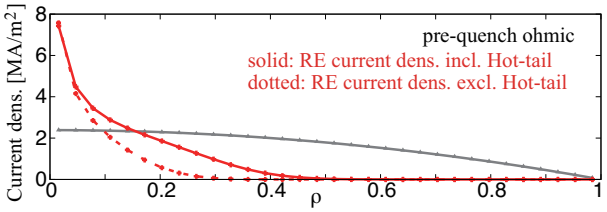

Figure 6. Current density profile for $n_e^f(0) = 1.2 \times 10^{21}$ m^{-3}.

collisionality.

Owing to the presence of earlier seed REs, the secondary RE generation is also triggered earlier. On axis, due to the RE generation in the earlier time, the electric field is also reduced earlier ($t \sim 15$ ms) and then the secondary RE generation is ended before $t = 30$ ms (the electric field satisfies $E/E_C < 1$ at the time). As a result, the total RE current density on axis becomes similar to that without H-T effect. At $\rho = 0.3$, on the other hand, since the primary RE generation rate at the first additional peak ($t \sim 5$ ms) is sufficiently greater than that at the subsequent peak, the secondary RE current density also becomes greater in spite of the earlier reduction of the electric field.

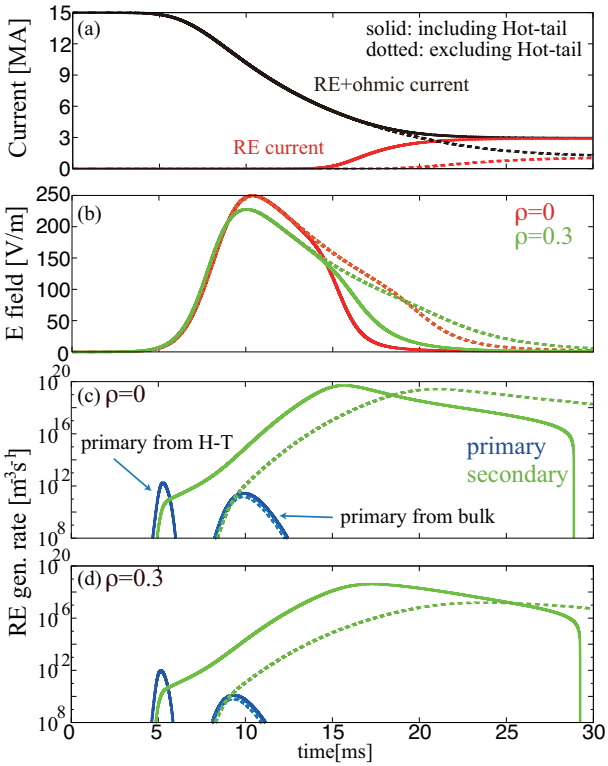

Figure 7. Evolutions of (a): Total and RE current, (b,c): electric field on $\rho = 0$ and $\rho = 0.3$, and (d,e): primary and secondary RE generation rates.

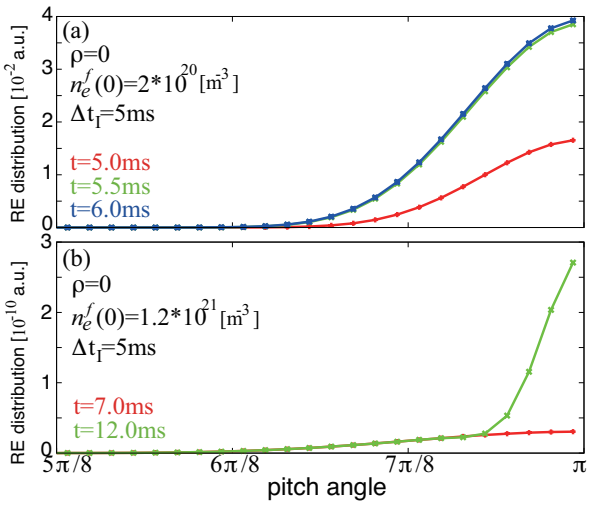

Figure 8. Cumulative primary RE momentum distribution, whose kinetic energy is 1.5MeV, versus pitch angle at several time steps on $\rho = 0$ for (a): $n_e^f(0) = 2 \times 10^{20}\mathrm{m}^{-3}$ and (b): $n_e^f(0) = 1.2 \times 10^{21}\mathrm{m}^{-3}$.

Consequently, RE current density around $\rho = 0.3$ is multiplied by the H-T effect and RE current density profile is broadened.

Figure 8 shows the pitch angle dependence of the cumulative primary RE

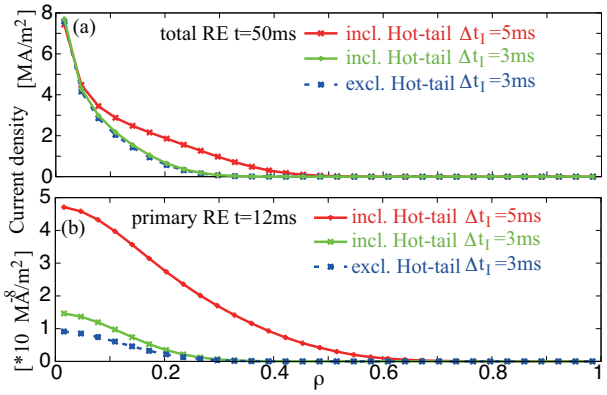

Figure 9. Radial profiles of (a): total and (b): primary RE current density for $\Delta t_{\rm I} = 5$ ms and 3 ms.

distribution for (a) $n_e^f(0) = 2 \times 10^{20}\mathrm{m}^{-3}$ and (b) $n_e^f(0) = 1.2 \times 10^{21}\mathrm{m}^{-3}$ cases. In higher density case, RE distribution at $t = 7$ ms consists of H-T RE generation (first peak) mainly and the increment of that at $t = 12$ ms consists of bulk primary RE generation (second peak). From fig. 8-(b), it is found that REs generated by the second peak of the primary RE generation are more localized around $\theta = \pi$ than those generated by the first peak. This is because H-T electrons have more perpendicular momentum than bulk electrons and they become REs keeping its perpendicular momentum. As a consequence, RE distribution in the pitch angle direction becomes a sum of the two kind of shapes. On the contrary, in the lower density case (namely fig. 8-(a)), since the most of REs are generated from H-T electrons, RE distribution has a single component which is not localized around $\theta = \pi$.

These results show that the presence of the first additional peak of the primary RE generation ($t \sim 5$ ms) multiplies the total RE current. Since $\Delta t_{\rm I} = 5$ ms is chosen in this result, the H-T REs start to be generated before the electron density reaches to post-injection density n_e^f. Therefore, next, $\Delta t_{\rm I} = 3$ ms is chosen to investigate the behavior of the H-T RE generation peak.

3.2. $\Delta t_{\rm I} = 3ms$ *case*

Figures 9 and 10 show the RE current density profiles and RE generation rates for $\Delta t_{\rm I} = 3$ and 5 ms with $n_e^f(0) = 1.2 \times 10^{21}$ m^{-3}. It is found that the faster increase of the electron density achieves to suppress the H-T RE generation in the whole plasma owing to the reduction of E/E_D until H-T RE generation starts as shown in figure 11. Contrary to the H-T RE generation, there is no difference in the bulk primary RE generation in both cases. This is because the bulk primary RE generation begins after $t \sim 8$ ms and E/E_D during $5 < t < 12$ ms (the bulk RE generation occurs in this duration) is nearly same between two cases as shown in fig. 11. The primary RE generation is sensitive to E/E_D [35, 38] and it is also sensitive to n_e via E_D. Since the H-T RE generation and the bulk primary RE generation occur in different time, the

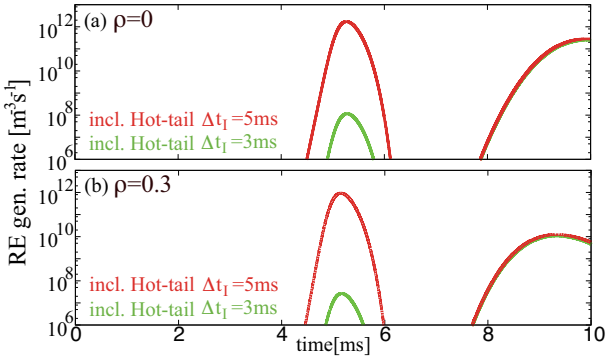

Figure 10. Primary RE generation rate on axis and $\rho = 0.3$ for $\Delta t_{\rm I} = 5$ ms and 3 ms.

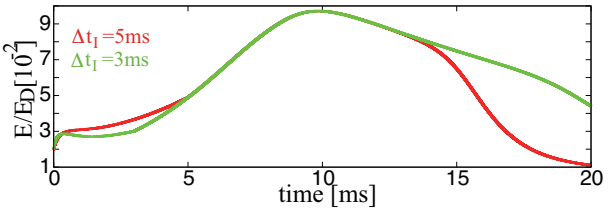

Figure 11. Evolutions of E/E_D on axis for $\Delta t_{\rm I} = 5$ ms and 3 ms.

Table 2. Generated RE current for $\Delta t_{\rm I} = 3$ ms and 5 ms cases at $t = 50$ ms.

	tot. RE	primary RE
$\Delta t_I = 5$ ms, on H-T	2.90MA	52.8 mA
$\Delta t_I = 5$ ms, off H-T	1.09MA	3.28 mA
$\Delta t_I = 3$ ms, on H-T	1.18MA	5.25 mA
$\Delta t_I = 3$ ms, off H-T	1.09MA	3.35 mA

degree of the RE suppression due to the increment of n_e is different in each generation. Therefore, in general, the H-T RE generation, which occurs earlier in time than the other RE generation, is difficult to be suppressed relatively by impurity injection.

Consequently the total RE current for $\Delta t_{\rm I} = 3$ ms is reduced to that excluding H-T effect as shown in fig. 9-(a). The generated RE current in both cases including/excluding H-T effect are listed in Table 2.

In the present models, we assume that the bulk temperature evolves independent on the electron and impurity density. The fast rise of the electron and impurity density, however, may shorten the thermal quench and enhance the H-T effect. Therefore, the accurate discussion of the H-T RE suppression by impurity injection requires to take the influence of the density rise to the thermal quench into account.

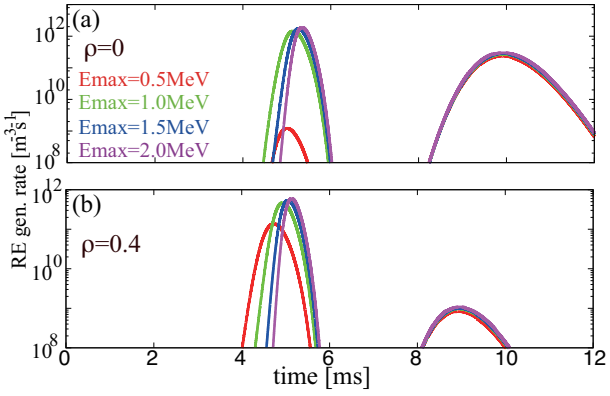

Figure 12. Primary RE generation rate with $\Delta t_{\mathrm{I}} = 5$ for several $E_{\max}$.

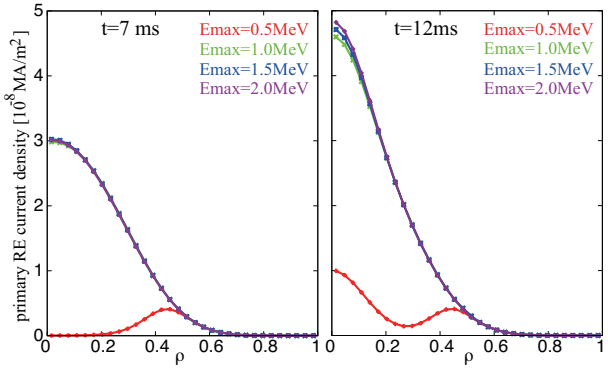

Figure 13. Primary RE current density profiles at (a) $t = 7$ ms and (b) $t = 12$ ms for several $E_{\max}$.

4. Validity of $E_{\max}$

The validity of the choice of $p_{\max}$, namely $E_{\max}$, in eq. (4) was already discussed in Ref. [28]. In the previous paper, it was shown that the primary RE current is insensitive to the choice of $E_{\max}$ and we chose $E_{\max} = 0.5$ MeV. In present simulations with high electron density ($n_e^f(0) \sim 10^{21}$ m^{-3}), however, we should choose $E_{\max} = 1.5$ MeV instead of 0.5 MeV. This is because that since the total primary RE current is too small and the pre-quench temperature is sufficiently high, the contribution of H-T RE generation from H-T electrons, whose kinetic energy is in the range of 0.5 MeV $< E <$ 1.5 MeV, can not be neglected as compared to the total primary RE current.

Figure 12 shows the primary RE generation rate (a) on axis and (b) $\rho = 0.4$ with $\tau_q = 1$ ms, $\Delta t_{\mathrm{I}} = 5$ ms, and $n_e^f(0) = 1.2 \times 10^{21}$ m^{-3} for several $E_{\max}$. From these figures, it is found that the peak value of the primary RE generation rate from H-T electron ($t \sim 5$ ms) with Emax $= 0.5$ MeV is smaller than those of $E_{\max} = 1.0$, 1.5, and 2.0 MeV cases especially on axis. Additionally, figure 13 shows that the primary RE current density profiles at $t = 7$ ms and 12 ms for several $E_{\max}$. The primary RE current at $t = 7$ ms consists of the RE current generated from H-T electrons as shown in fig. 12

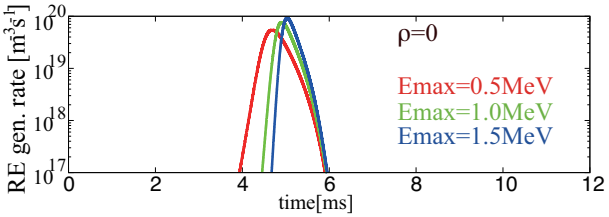

Figure 14. Evolutions of the primary RE generation rate on axis for $E_{\max} = 0.5$, 1.0, and 1.5 MeV with $n_e^f(0) = 2 \times 10^{20}$ m^{-3}, $\tau_q = 1$ ms, and $\Delta t_{\rm I} = 5$ ms.

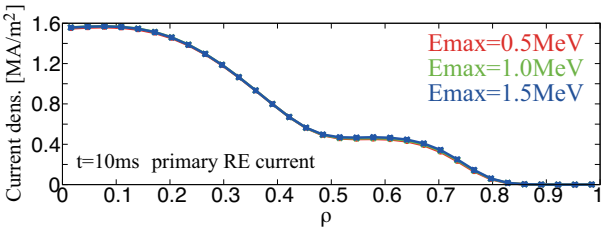

Figure 15. Primary RE current density profiles at $t = 10$ ms for $E_{\max} = 0.5$, 1.0, and 1.5 MeV.

and that at $t = 12$ ms is total (H-T and bulk) primary RE current. From fig. 13, it is found that the primary RE current from H-T electrons is sensitive to the value of $E_{\max}$, if the value of $E_{\max}$ is less than 1.0 MeV. For $n_e^f(0) = 1.2 \times 10^{21}$ m^{-3} case, the primary RE current at $t = 7$ ms becomes 10.6 mA ($E_{\max} = 0.5$ MeV), 46.9 mA ($E_{\max=1.0}$ MeV), 46.7 mA ($E_{\max} = 1.5$ MeV), and 46.4 mA ($E_{\max} = 2.0$ MeV) and the total primary RE current becomes 15.6 mA, 52.7 mA, 52.8 mA, and 52.9 mA, respectively.

H-T RE current density in the case with $E_{\max} = 0.5$ MeV is underestimated especially in inner region ($\rho < 0.4$). This underestimation comes from the fact that there are non-negligible number of H-T electrons in the range of 0.5 MeV $< E_{\max} <$ 1.5 MeV because of the high electron temperature in the inner region. Since the contribution of such H-T electrons to RE generation is omitted in the case with $E_{\max} = 0.5$ MeV, RE current density is underestimated. Although the RE current generated from such H-T electrons is tens of mili amperes, the contribution can not be neglected because the primary RE generation from $E < 0.5$ MeV region is further small (~ 10.6 mA).

Figure 14 shows the evolutions of the primary RE generation rate for $E_{\max} = 0.5$, 1.0, and 1.5MeV with $n_e^f(0) = 2 \times 10^{20}$ m^{-3}, $\tau_q = 1$ ms, and $\Delta t_{\rm I} = 5$ ms. Additionally, figure 15 shows the radial profile of the primary RE current density at $t = 10$ ms for several $E_{\max}$ cases. In this case, since the primary RE generation from the range of $E < 0.5$ MeV is sufficiently large to neglect the contribution from 0.5 MeV $< E$, the primary RE generation is insensitive to the choice of $E_{\max}$.

From the discussion in this section, we can see that the primary RE generation is insensitive to the boundary value of momentum space if the boundary value $E_{\max}$ is greater than 1 MeV in present simulation parameters. In this reason, we chose

$E_{\max} = 1.5$ MeV as a boundary value.

5. Conclusion

We have applied the two-dimensional Fokker-Planck simulation to describe the RE generation including the H-T effect in disruptions with impurity injection. We have confirmed that the RE generation is suppressed with the increase of the electron density. If the H-T effect is not taken into account, the RE current is reduced from $I_{\rm RE} \sim 12$ MA ($n_e^f(0) = 2 \times 10^{20}$ m^{-3}) to ~ 1 MA in the high density region ($n_e^f(0) = 1.2 \times 10^{21}$ m^{-3}). If the H-T effect is included, the H-T effect multiples the primary RE current $I_{\rm prim}$. In low density case ($n_e^f(0) = 2 \times 10^{20}$ m^{-3}), H-T effect has less influence to the total RE current in spite of the increase of the primary RE generation ($\Delta I_{\rm prim} \sim 0.9$ MA), since the much more primary RE current reduces the electric field and the secondary RE current. In high density case ($n_e^f(0) = 1.2 \times 10^{21}$ m^{-3}), on the other hand, the H-T effect multiplies the primary RE current slightly ($\Delta I_{\rm prim} \sim 50$ mA). Despite of the small increment of the primary RE current, total RE current is tripled ($I_{\rm RE} = 1.09 \rightarrow 2.90$ MA) due to the avalanche effect. This multiplication of RE current comes from the H-T RE generation, which is triggered in the earlier time ($t \sim 5$ ms) than the bulk primary RE generation ($t \sim 10$ ms). If the electron density increases up insufficiently until the H-T RE generation starts, the H-T effect can generate non-negligible primary RE current. Conversely, it is also confirmed that sufficiently faster increase of the electron density may suppress the H-T RE generation.

The present simulation study makes clear that the H-T effect is important for the RE generation with short thermal quench even in high electron density plasma. There is a possibility that the impurity injection operation planned for ITER operation to avoid the RE generation in disruptions shortens the thermal quench duration and invokes the H-T effect, which may produce non-negligible primary RE current and large secondary RE current. Conversely, if the increase of the electron density is sufficiently faster than H-T RE generation, impurity injection may suppress the H-T effect. From these results, reliable estimation of the thermal quench, the evolution of the electron density by impurity injection, and impurity transport is inevitable for the estimation of RE current.

Acknowledgment

This study was supported in part by the Grant-in-Aid for scientific research, No. 23246163 and 26289356, from Japan Society for the Promotion of Science, and by the use of the Helios system at the International Fusion Energy Research Center (project code: FPSREG). This work is also performed on "Plasma Simulator" (FUJITSU FX100) of NIFS with the support and under the auspices of the NIFS Collaboration Research program (NIFS16KNSR005).

[1] T. Hender, J. Wesley, J. Bialek, et al.: Nuclear Fusion **47** (2007) S128.

[2] N. Commaux, L. R. Baylor, S. K. Combs, et al.: Nuclear Fusion **51** (2011) 103001.
[3] E. Hollmann, P. Aleynikov, T. Fülöp, et al.: Physics of Plasmas **22** (2015) 021802.
[4] M. Lehnen, S. Bozhenkov, S. Abdullaev, et al.: Physical review letters **100** (2008) 255003.
[5] N. Eidietis, N. Commaux, E. Hollmann, et al.: Physics of Plasmas **19** (2012) 056109.
[6] R. Granetz, B. Esposito, J. Kim, et al.: Physics of Plasmas **21** (2014) 072506.
[7] V. Riccardo, P. Andrew, L. Ingesson, et al.: Plasma physics and controlled fusion **44** (2002) 905.
[8] M. Bakhtiari, Y. Kawano, H. Tamai, et al.: Nuclear fusion **42** (2002) 1197.
[9] D. Whyte, T. Jernigan, D. Humphreys, et al.: Journal of nuclear materials **313** (2003) 1239.
[10] G. Martin, F. Sourd, F. Saint-Laurent, et al. Disruption Mitigation on Tore Supra. Proc. of 20th IAEA FEC (Villamoura, 2004). (Vienna:IAEA) CD-ROM file EX/10-6Rc.
[11] E. Hollmann, T. Jernigan, M. Groth, et al.: Nuclear fusion **45** (2005) 1046.
[12] R. Granetz, E. Hollmann, D. Whyte, et al.: Nuclear Fusion **47** (2007) 1086.
[13] G. Pautasso, C. Fuchs, O. Gruber, et al.: Nuclear Fusion **47** (2007) 900.
[14] R. Yoshino, T. Kondoh, Y. Neyatani, et al.: Plasma physics and controlled fusion **39** (1997) 313.
[15] P. Taylor, A. Kellman, T. Evans, et al.: Physics of Plasmas **6** (1999) 1872.
[16] N. Commaux, L. R. Baylor, T. C. Jernigan, et al.: Nuclear Fusion **50** (2010) 112001.
[17] E. Hollmann, N. Commaux, N. Eidietis, et al.: Physics of Plasmas **17** (2010) 056117.
[18] R. Harvey, V. Chan, S. Chiu, et al.: Physics of Plasmas **7** (2000) 4590.
[19] H. Smith, P. Helander, L.-G. Eriksson, et al.: Physics of Plasmas **12** (2005) 122505.
[20] S. Chiu, M. Rosenbluth, R. Harvey, et al.: Nuclear Fusion **38** (1998) 1711.
[21] H. Smith, E. Verwichte: Physics of Plasmas **15** (2008) 072502.
[22] T. Fehér, H. Smith, T. Fülöp, et al.: Plasma Physics and Controled Fusion **53** (2011) 035014.
[23] A. Stahl, O. Embréus, G. Papp, et al.: Nuclear Fusion **56** (2016) 112009.
[24] V. Plyusnin, V. Riccardo, R. Jaspers, et al.: Nuclear Fusion **46** (2006) 277.
[25] L. Zeng, H. R. Koslowski, Y. Liang, et al.: Journal of Plasma Physics **81** (2015).
[26] H. Nuga, A. Matsuyama, M. Yagi, et al.: Journal of Plasma and Fusion Research **10** (2015) 1203006.
[27] H. Nuga, A. Matsuyama, M. Yagi, et al.: Journal of Plasma and Fusion Research **11** (2016) 2403023.
[28] H. Nuga, M. Yagi, A. Fukuyama: Physics of Plasmas **23** (2016) 062506.
[29] Y. Sokolov: JETP Letters **29** (1979) 218.
[30] R. Jayakumar, H. Fleischmann, S. Zweben: Physics Letters A **172** (1993) 447.
[31] M. N. Rosenbluth, S. V. Putvinski: Nuclear Fusion **37** (1997) 1355.
[32] C. Karney: Computer Physics Reports **4** (1986) 183.
[33] C. F. F. Karney, N. J. Fisch: Phys. Fluids **28** (1985) 116.
[34] J. Wesson: *"Tokamaks 3rd Edition"* (Oxford University Press, 1987).
[35] J. W. Connor, R. J. Hastie: Nuclear Fusion **15** (1975) 415.
[36] I. P. B. Editors: Nuclear Fusion **39** (1999) 2251.
[37] E. Hollmann, T. Jernigan, P. Parks, et al.: Nuclear Fusion **48** (2008) 115007.
[38] H. Dreicer: Physical Review **115** (1959) 238.